EASR

Engineering and Applied Science Research

https://www.tci-thaijo.org/index.php/easr/index

Published by the Faculty of Engineering, Khon Kaen University, Thailand

Investigation of shear strength and metallurgy on semi-solid metal 356 aluminium alloy with lap joint by friction stir spot welding

Chaiyoot Meengam*[1)], Suppachai Chainarong[1)] and Siva Sitthipong[2)]

[1)]Faculty of Industrial Technology, Songkhla Rajabhat University, Songkhla 90110, Thailand
[2)]Industrial Metrology and Testing Service Center, Thailand Institute of Scientific and Technological Research, Samut Prakan 10280, Thailand

Received 12 December 2020
Revised 30 April 2021
Accepted 3 May 2021

Abstract

The SSM 356 aluminum alloy formed by GISS technique, which was developed to be used in the production of automobile parts and necessary for FSSW process, is found to be good adhesion of the lap joint. The results of all experiments were very satisfying. For rotation speed at 380 rpm, the plug depth of 1.5 mm and the welding time of 60 sec, the maximum shear strength was 174.2 MPa, whose Joint efficiency was 92.12 percent compared with the base metal. The values of hardness in SZ ranged lower than those in other regions, while the hardness values in the advancing side of thermo-mechanically affected zone (AS-TMAZ) were higher than those in other regions. The evaluation of the microstructure in SZ shows that external force and heat cause the material to become plastic deformation resulting in the new precipitations from β-Mg_2si phase to β″-Mg_2si homogenous phase whose particle size is smaller around 2-7 µm. The analyzed experimental design was a general mixed-level design which had a test coefficient of R^2 of 0.96 at confidence level of 95.00%.

Keywords: Friction stir spot welding, SSM 356 aluminium alloy, Shear strength, Joint efficiency, Globular structures

1. Introduction

The wrought aluminum alloy grade of A356 is commonly used in many industries because of its lightweight, corrosion-resistance, and good mechanical properties according to Chainarong et al. [1]. The aluminum forming process is used in the automotive industry, especially in the automotive parts manufacturing such as engine bracket, gear housing, gear cover, and steering wheels including casting methods, as stated in Chen et al. [2]. Currently, the aluminum casting process is greatly improved as to reduce waste after the process and shows effective cost controlling capabilities in the production process. In addition, the semi-solid aluminum casting technology is another technique used for modern castings and it is currently being used in the production of automotive parts. For this research, the 356 semi-solid aluminum alloys were produced by the semi-solid casting with Gas Induced Semi-solid technique (GISS) as mentioned in Wannasin et al. [3]. With such material, the engineers could design these car parts very easily for maintenance and safety. Therefore, the welding methods and joints of the design are important. Yang et al. [4] found that the spot welding is another method used to weld car during assembly line due to having a positive effect on welding quality. However, the friction-stir-spot welding method (FSSW) has also been used for automotive assembly due to being environmentally friendly, good quality of joints, and low welding cost mentioned in Chong Gao et al. [5]. The joint welding of FSSW is more popular to be designed for lap joint than other types. The FSSW is a solid-state welding method, developed from friction stir welding in the Welding Institute in Great Britain (TWI) in UK in 1991. [6]. Rao et al. [7] showed that the quality of the joint strength is derived from the welding parameters. These affect the heat input into welding, which significant parameters of the FSSW are rotation welding speed, welding time, and depth of plunge. Especially, Wenya Li et al. [8] discovered that defects, also called “hook”, are generated by welding parameters. Heat input during FSSW process is an important cause for a hook, which directly affects the mechanical properties. Moreover, Tozaki et al. [9] revealed that the tool probe affects the mechanical properties and the microstructure. Because fine grain structures and coarse grain structures can be found next to the tip of the tool probe. However, the welding parameters of the FSSW that affect the change of microstructure and mechanical properties after welding are rotation speed, welding time, depth of plunge, down force, depth rate, smoothness of surface, cleanliness of weld surface, or even the shape of the welding tool according to Sitthipong et al. [10]. The mechanism of FSSW causes heat which is generated on the surface of the sample with a tool shoulder until the material becomes soft (plastic deformation behavior). The tool pin drags and stirs the material, resulting in the material welded together (Huijie Liu et al. [11]). Although the specimen after FSSW had a groove (keyhole) at the joint, which was caused by the tip of the welding tool (Fereiduni et al. [12]), samples after FSSW still maintain desirable mechanical properties. In addition, the welding cost is an important factor of industry decisions as it is certainly what the industry needs. Cost evaluation with accurate equations can reduce wasteful experiments. Lakshminarayanan et al. [13] solved the concern with different parameters in the experimental design and were able to reduce

*Corresponding author. Tel.: +66 7426 0200
Email address: Chaiyoot.me@skru.ac.th
doi: 10.14456/easr.2022.18

insignificant parameters into account. Finite Element (FEM) analysis FSSW was used to forecast the friction heat until the samples reach the desired mechanical properties after welding by Urso et al. [14].

For this research, our team was interested in studying different parameters of FSSW on novel materials from a semi-solid casting by GISS method. The sample of SSM 356 aluminium alloy after FSSW was compared with the shear strength of base metal and calculated the joint efficiency. Moreover, the parameters affecting shear strength was predicted using regression equation with statistical method analysis. The research studied the hardness properties at the stir zone (SZ), thermal mechanical affect zone (TMAZ), and base metal (BM). The transformation of globular structures in SZ and microstructure in other areas was evaluated by an optical microscope (OM), a scanning electron microscope (SEM), and an Energy-dispersive X-ray spectroscopy (EDS) in order to characterize distribution of particles. The experiment results will be evaluated and shown further.

2. Materials and methods

The main purpose of the research is to investigate the effects on the rotation welding speed, the depth of plunge and the welding time caused by changes of globular structures of SSM 356 aluminum alloy. Also, a new technique for GISS process was developed for semi-solid casting. The deformation of the microstructure in the heat-affected area is interesting to be investigated. Especially, the changes in microstructure will lead to differences in mechanical properties after welding. Moreover, a mathematical equation to determine the shear strength will be shown in this research; meanwhile, the regression equation will accurately predict the next FSSW of SSM 356 aluminum alloy.

2.1 GISS 2024 aluminum alloy

The materials in this experiment was the SSM 356 aluminum alloy, formed by the semi-solid casting using the GISS technique, which was supported by GISCO Company Limited. As described by Burapa et al. [15], the ingot of 356 aluminum alloy was melted by an electric furnace at 640 ºC for up to 6 hours. After that, nitrogen gas was injected via a porous graphite diffuser with the rate of 9 liters per minute via porous graphite by the time at quenching was obtained for 10 sec following by squeeze casting respectively. The activity force of nitrogen gas destroys the dendrite structure forming many globular structures with the grain size around 20-25 µm. The microstructure of SSM 356 aluminum alloys includes aluminum matrix (α-Al) and Mg_2Si from eutectic phase shown in Figure 1. The chemical compositions of this alloy are listed in Table 1, and the mechanical properties are listed in Table 2.

Table 1 Chemical composition of SSM 356 aluminum alloy

Materials	Si	Fe	Cu	Mn	Mg	Zn	Ti	Al
356	7.74	0.57	0.05	0.06	0.32	0.01	0.05	Bal.

Table 2 Mechanical properties of SSM 356 aluminum alloy

Ultimate tensile strength (MPa)	Elongation (mm)	Hardness Vickers (HV_{10})
189	14	67

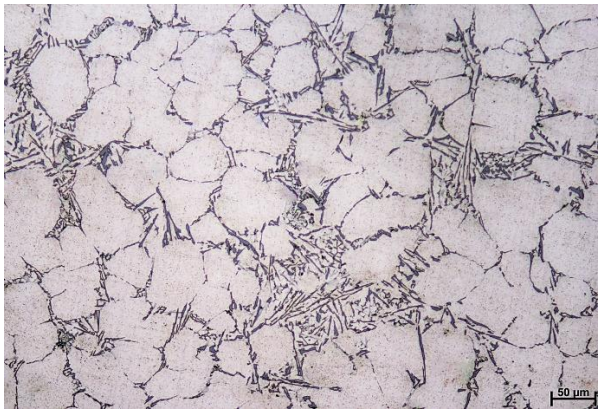

Figure 1 The globular microstructures of SSM 356 aluminum alloy

2.2 Friction stir spot welding step

In the experiment, the sample of 4 mm thick aluminum sheets with a dimension of 28x95 mm was prepared. The tool used in the FSSW process was made from H13 tool steel, which was formed as a cylindrical profile with a dimension of 15 mm in width, tool pin of 5 mm, and 3.2 mm long respectively. The steps of FSSW for SSM 356 aluminum alloy are described as follows: 1) The samples were clamped firmly by jigs by designed to prevent heat input during welding from the samples to the jigs, are also important for FSSW because the heat generated during welding could directly affect the softening process of the welding material. The protection with thermal insulation materials is therefore used in this research. 2) The stationary side was controlled in a clockwise direction. 3) Then, the samples were placed as lap joint welding with an overlap at 28 mm shown in Figure 2. At the end of the tool, it was positioned in the middle of the joint, and pressure was applied to the surface of the tool shoulder on the sample's surface. The tool was pressed and traveled onto the sample surface at a speed of $0.125x10^2$ mm/min. When the shoulders of the tool touch the sample surface, it will be pressed until reaching the depth of plug according to the specified parameters. At that time, the heat was generated from friction force between the tool shoulder and the surface of samples. 4) Finally, heat causes the material to become soft and the material flows in

around the tool pin. This will lead to a complete welding while maintaining an appropriate welding time. The sample after using FSSW had a keyhole at the joint, which was caused by the tip of the welding tool. The condition in the experiment are listed in Table 3. The schematic of FSSW of SSM 356 aluminium alloy is presented in Figure 3.

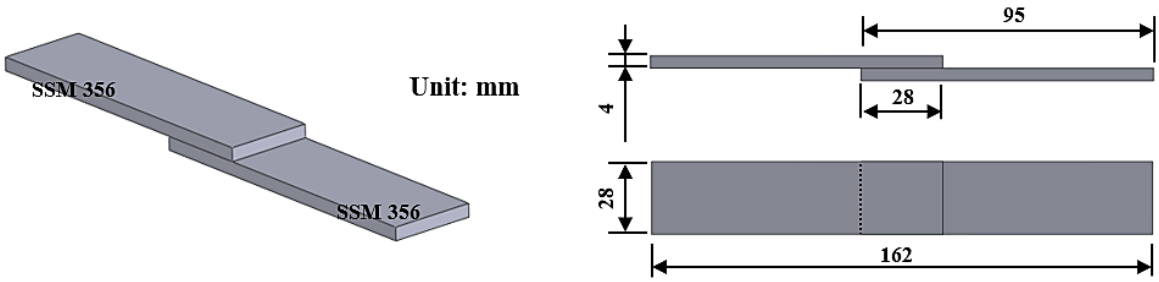

Figure 2 Lap joint of FSSW of SSM 356 aluminum alloy

Table 3 The parameters in the experiment of FSSW of SSM 356 aluminum alloy

Process parameters	Unit	Values
Rotation speed	rpm	380, 1240 and 2500
Depth of plug	mm	1.0 and 1.5
Welding time	sec	30 and 60
Tool shoulder diameter	mm	15
Tool pin diameter	mm	5
Tool pin length	mm	3.2
Depth rate	mm/min	$0.125x10^{2}$
Tool shape	---	Cylinder

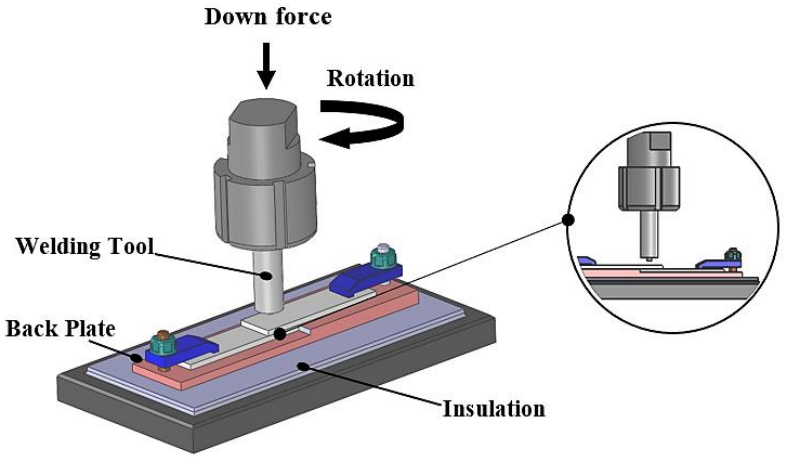

Figure 3 Lap joint of FSSW of SSM 356 aluminum alloy

2.3 Design of the experiments

The preliminary parameters in the experiments affect the bonded strength of samples, and then set the parameters for the experiment. The parameters in this experiment were shown in Table 4 and each test was repeated 3 times. Thus, the total number of experiments were 32 experiments and they were general mixed level design.

Table 4 The parameters and levels for the design of experiments in general mixed level design

Parameters	Levels
Rotation speed (*Rs*)	380, 1240 and 2500 rpm
Depth of plug (*Dp*)	1.0 and 1.5 mm
Welding time (*Wt*)	30 and 60 sec

2.4 Mechanical testing

After FSSW process, the shear strength of the samples was tested under room temperature by following American Society for Testing of Materials by ASTM B769 standards [16]. This shear strength testing was conducted by a crosshead speed of $1.67x10^{-2}$ mm/sec with a universal testing machine LLOYD model EZ50. The results of the shear strength obtained from the tests were calculated for the joint efficiency and estimate the character of the joint surface after tensile testing. Finally, Vickers microhardness was conducted

on the Zwick/Roell model ZHU; the samples were tested for the total of 32 spots around the stir zone. The distance between testing spots was 0.2 mm apart. The pressure test was 10 HV and dwell time for 10 sec with a pyramid square diamond probe and a tip angle of 136 degrees respectively.

2.5 Metallurgy analysis

The samples were prepared for microstructure changes and defects examination. The SiC papers at P180, P320, P400, P600, P800, P1000, and P1200 grit were used to polish on the surface of the samples respectively. Then, they were polished with alumina powder with the particle size at 5, 3, and 1 μm, and etched with Keller's reagent. After sample preparation, the macrostructure was evaluated by a Zeiss Stemi DV4 Stereo Microscope. Microstructure changes and defects were observed by a light optical microscope with Olympus model BH2-UMA. At the same time, for distribution of the particles, quantitative chemical composition analysis was performed by an electron microscope on the FEI-Quanta model 450 FEG and element analysis with Oxford Instruments model X-Max 50, which was supported by Thaksin University.

3. Results and discussion

3.1 Shear strength results

The shear strength of SSM 356 aluminium alloy with lap joints welded by FSSW method is shown in Figure. 4. The experiment results show that the samples obtained good strength after welding. The lower rotation speed and depth of plug it was, the better shear strength it was observed. This is because the increase of depth of plug creates more heat and plastic flow of material during welding. However, at high rotation speed, it can be reduced shear strength. For example, the shear strength at 2500 rpm tends to be decreased because the heat accumulation causing excessive amounts of flash. Therefore, the heat energy will be different depending on the experimental conditions. The heat is calculated by the following equation q0 (W/m^2).

$$q0 = \pi d \mu p N \quad (1)$$

When π is the constant, d is a diameter of the tool (mm), μ is the dynamic friction coefficient (μ = 0.6 in this work), p is a contact pressure (Pa) or depth of plug (mm), and N is a rotating speed [7] respectively. However, other parameters directly relate to the heat generation. For example, the increasing diameter of tool shoulder results in the increasing heat as well. For the rotation speed at 380 rpm, depth of plug at 1.5 mm, and welding time 60 sec, the maximum average shear strength value was 174.2 MPa. Compared with the shear strength of base SSM 356 aluminium alloy at 189.0 MPa, the joint efficiency of such condition was 92.12 percent. On the other hand, for the rotation speed at 380 rpm, depth of plug at 1 mm, and welding time 30 sec, the minimum average shear strength value was 106.9 MPa or around 56.56 percent of joint efficiency [17].

$$\text{Joint efficiency} = \frac{\text{Shear strength of FSSW samples}}{\text{UTS of base SSM 356 aluminium alloy}} \times 100 \quad (2)$$

For rotation speed at 1240 and 2500 rpm, depth of plug at 1.0 mm, and welding time 30 sec, their shear strength values were 113.1 (60.8 percent of joint efficiency) and 118.3 MPa (62.6 percent of joint efficiency) respectively. For rotation speed at 1240 and 2500 rpm, depth of plug at 1.5 mm, and welding time 60 sec their shear strength values were 156.0 (82.5 percent of joint efficiency) and 117.4 MPa (62.1 percent of joint efficiency) respectively. However, joint efficiency also resulted from other factors, especially the presence of defects, such as flash, kissing bond, void, cavity or groove, cracks, residual stress, and hook [18]. These defects will cause the joints to become weak which could affect the mechanical properties. Moreover, residual stress after FSSW could affect joint efficiency. Cooling rate causes residual stress in the SZ [19]. The characteristic of microstructure after FSSW directly affects joint efficiency. The new recrystallization of the structure, resulting in the new formation of atoms, makes the quality of the joint become different [20]. For other parameters, the shear strength can be considered from the Figure. 4.

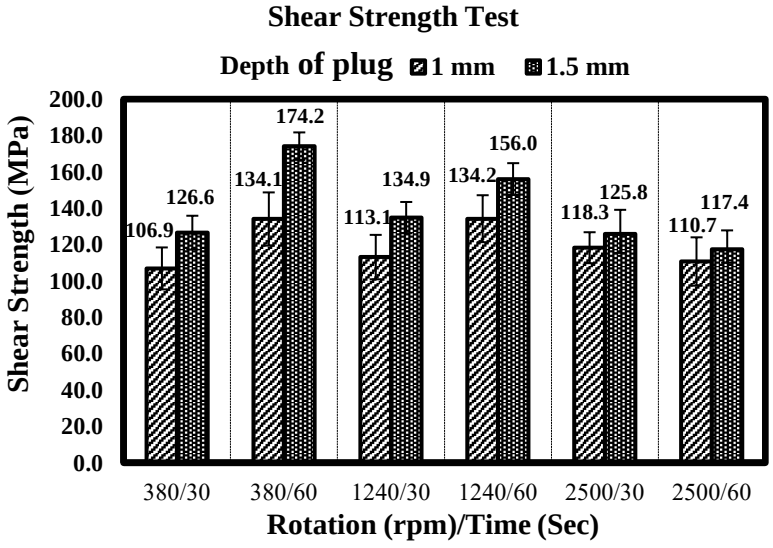

Figure 4 The shear strength of FSSW of SSM 356 aluminium alloy

3.2 Statistical method analysis of model accuracy results

The accuracy of the obtained data was checked before further analysis. After data normalization, it was found that three factors affected the shear strength, namely the rotation speed, depth of plug, and welding time. The data validation can be considered from the following reasons. First, data was normally distributed, and the normal probability plot was along a straight line. Second, data in Versus Fits plot show an independent distribution because no clear evidence of group formation. Third, data showed stability of variance because the plots were randomly distributed; thus, this data was fit for probability analysis presented in Figure 5.

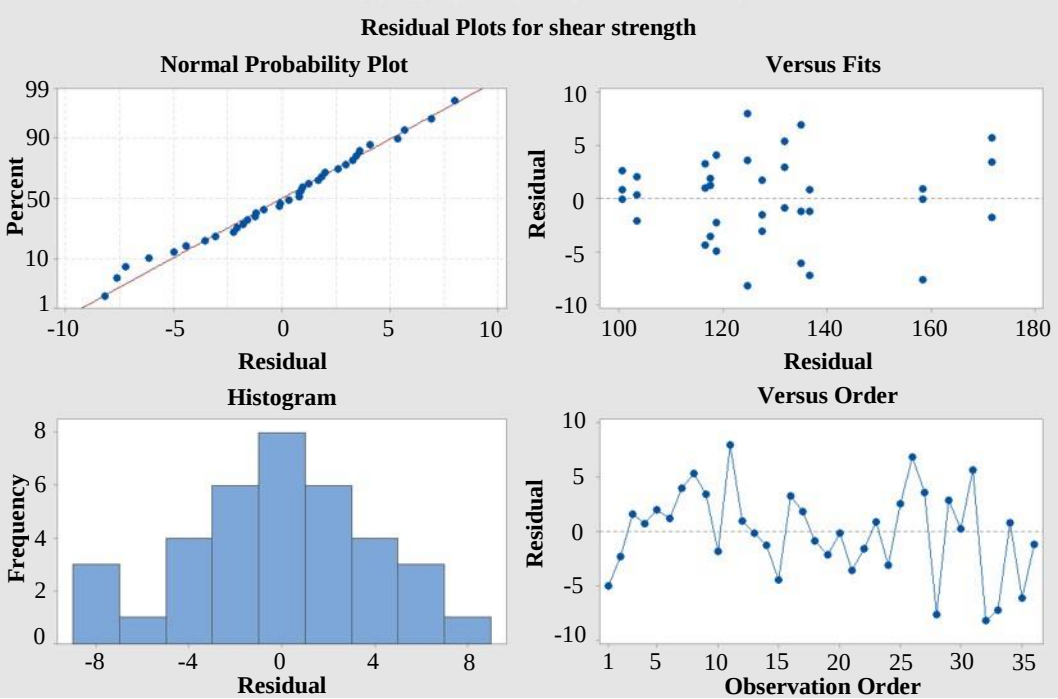

Figure 5 The graphical model of the data accuracy checking

In order to find the relationship among experimental factors, the data were analyzed for variance. According to the shear strength results, it was found that there is variation among rotation speed, depth of plug and welding time at 95.00% confidence level. Also, coefficient of determination R^2 was 0.96 and adjusted R^2 was 0.95 respectively. Therefore, this factorial design model can be used to precisely predict the shear strength from FSSW of SSM 356 aluminum alloys as shown in Table 5.

The factors in this experiment are used as the mathematical equation, which corresponds to the lack of fit test and the high p-value clearly shows that the experimental model is accurate from the data used in the prediction.

$$\text{Shear strength} = -0.7 + 0.07538Rs + 0.967Dp + 45.3Wt - 0.000008Rs^2 - 0.000806RsDp - 0.01984RsWt + 0.54DpWt \quad (3)$$

The surface plots of shear strength are shown in Figure 6. The plots show that the higher rotation speed causes higher shear strength. The high rotation speed causes overheating and too much flash in weld zone. High residual stress and structural transformation in SZ can decrease the shear strength, presented in Figure 6(a). In contrast, the depth of plug and welding time show an opposite effect on the rotation speed. It was found that lower depth of plug and welding time affect the fracture of β-Mg_2si particles causing the low shear strength, presented in Figure 6(b and c).

Table 5 The parameters in the experiment of FSSW of SSM356 aluminum alloy

Source	DF	Adj SS	Adj MS	F-Value	P-Value	
Regression	7	13960.1	1994.3	100.52	0.000	Significant
Rs	1	2564.4	2564.4	129.25	0.000	
D*p*	1	266.1	266.1	13.41	0.001	
W*t*	1	370.2	370.2	18.66	0.000	
Rs^2	1	581.3	581.3	29.30	0.000	
Rs D*p*	1	3991.0	3991.0	201.16	0.000	
Rs W*t*	1	671.6	671.6	33.85	0.000	
D*p* W*t*	1	147.6	147.6	7.44	0.011	
Lack of Fit	4	85.5	21.37	1.09	0.383	
Pure Error	24	470.0	19.58			
Total	35	14515.6				
R^2	0.96					
Adjusted R^2	0.95					

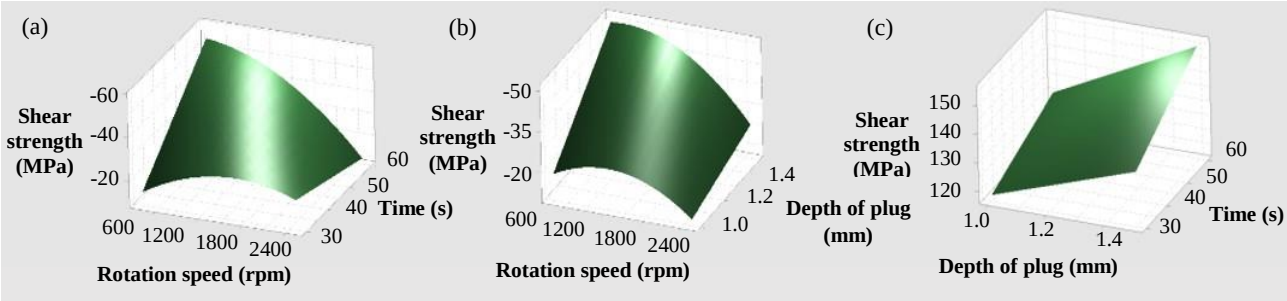

Figure 6 The contour plots for optimized of shear strength

In order to confirm the accuracy of regression equation, this equation has to be tested by using the response optimizer model to find the best conditions for the experiment with 5 replicates. To confirm the test results, the experiment was conducted under the conditions of rotation speed at 380 rpm, welding time at 60 sec, and 1.5 mm for depth of plug. The shear strength after testing were 168.7, 170.5, 169.4, 167.7 and 168.4 MPa respectively. All 5 values are in the forecasting range of response optimizer values (from 161.56 to 181.87 MPa). Moreover, the average shear strength was 168.94 MPa, which is in the forecasting range of response optimizer values (from 167.25 to 176.17 MPa) as shown in Table 6. In addition, forecasting the shear strength with mathematical equations by using finite element analysis can also be done [21].

Table 6 The prediction for shear strength of FSSW of SSM356 aluminum alloy

Prediction for shear strength				
Multiple response prediction				
Variables	Setting			
Rotation speed (rpm)	380			
Welding time (Sec)	60			
Depth of plug (mm)	1.5			
Response	Fit	SE Fit	95% CI	95% PI
Shear strength	171.71	2.18	167.25, 176.17	161.56, 181.87

3.3 Hardness results

Figure 7 shows results for vicker's hardness of SSM 356 aluminium alloy with lap joints welded by FSSW method. For hardness test, only 3 experiment results were presented due to the results of the experiment were similar. The rotation speed at 380 rpm, depth of plug at 1.5 mm, and welding time 60 sec provides lower hardness than rotation speed at 1240 and 2500 rpm. This is because the rotating speed affects the heat and can be explained by the heat equation. The experimental results showed that the hardness value of the thermo-mechanically affected zone from the advancing side (AS-TMAZ) was higher than other regions. The hardness values in this area were around 60-64 HV caused by the change of grain structure, resulting in the stress of grain while deforming [22], while the retreating side of thermo-mechanically affected zone (RS-TMAZ) with hardness values around 53-58 HV. It is worth to note that the stir zone (SZ) was found to have lower hardness than other regions because the SZ was at the end of the tool pin which hardness values were around 35-40 HV. Like what the result found in the rotation speed of 380 rpm, for the rotation speed at 1240 rpm, depth of plug at 1.5 mm, and welding time 60 sec shown in Figure 7(b), the AS-TMAZ showed the high hardness due to that region received heat distribution. This heat leads to a new precipitation of the microstructure while at the end of the welding tool is a region where the heat is not easily distributed. Figure 7(c) shows SZ region that had the lowest hardness ranging from 45-50 HV which was from the rotation speed at 2500 rpm, depth of plug at 1.5 mm, and welding time 60 sec. This was caused by the density of the material and heat distribution after different FSSW process. However, the hardness values from AS-TMAZ and RS-TMAZ were different after FSSW process. The hardness in AS-TMAZ values from 70 HV to 74 HV and in RS-TMAZ values from 67 HV to 70 HV respectively. The thermal coefficient of the material is another factor that supported the accumulation of heat at the SZ, which this heat accumulation could promote the increase of hardness [23].

3.4 Metallurgy results

3.4.1 Macrostructural results using a Zeiss microscopy

The macrographs were obtained at 10x magnification from the rotation speed at 380 rpm by Zeiss microscopy shown in Figure 8. It shows the comparison of depth of plug that affects the macrostructure in SZ. It can be observed that using the depth of plug at 1.5 mm produces more tear of the joint than using the depth of plug at 1 mm. This tear gap is caused by the rebounded-back behavior of the material from the action forced, affecting the width of the tear gap shown in Figure 8(a). However, the heat and the action force caused the rebound-back behavior and plastic deformation in the SZ. The heat is generated by friction in this area under the shoulders and around the pin. This friction was created from different parameters defined in FSSW shown in Figure 8(b). The heat generation also comes from shoulder sizes, thermal coefficient of the material and the movement of the circular circumference as

$$q0 = \frac{4}{3}\pi^2 \mu P \omega R^3 \quad (4)$$

When μ is the coefficient of friction, P is the compression force, ω is the circular motion, R is the radius of the shoulder and π is a constant [24].

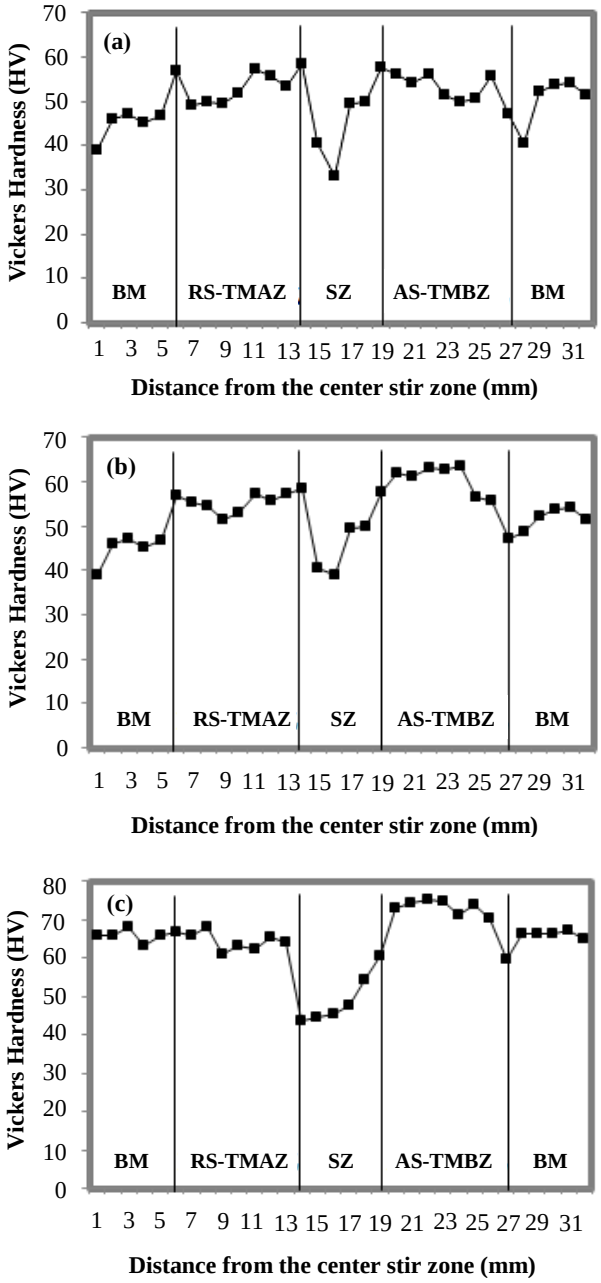

Figure 7 Hardness profiles across the weld region as: (a) rotation speed at 380 rpm, (b) rotation speed at 1240 rpm and (c) rotation speed at 2500 rpm

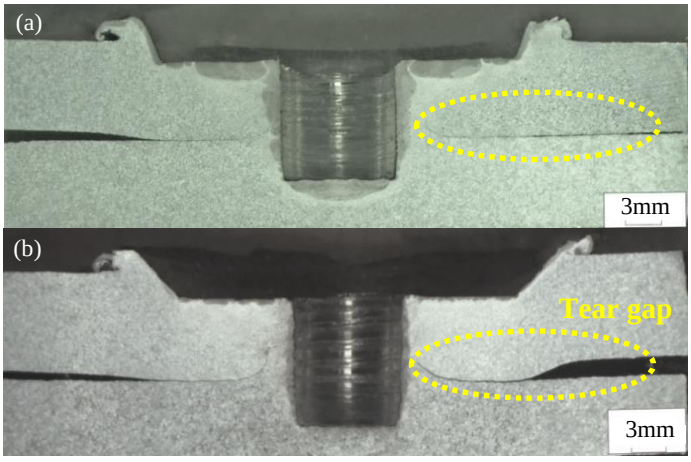

Figure 8 The macrostructure of rotation speed at 380 rpm, welding time 60 sec and depth of plug at (a) 1.0 mm and (b) 1.5 mm

3.4.2 Microstructural results using a light optical microscopy

Figure 9 shows the position of the microstructure examination, which was examined at 16 different points. The microstructure in SZ at 100x magnification by an optical microscope at rotation speed 380 rpm is shown in Figure 10. It was found that heat and force caused the globular structure to be deformed in the SZ by α-Al phase (Matrix phase) and crushed until become fine. Meanwhile, Mg_2Si phase (Eutectic phase) penetrated through the grain boundary, which was broken by mechanical action, resulting the precipitation of the structure in the SZ as shown in Figure 10 (a and b) [25]. In TMAZ, α-Al phase was heated until the size of the grain grew up. For AS-TMAZ, the material was dragged and caused the flow direction of the materials as the rotation pattern like a worm-like appearance. However, the hook was observed around the interface area between the upper sheet and the lower sheet because the heat and the force cannot be distributed into this region as shown in Figures 10(d). For RS-TMAZ, a new precipitation of the structure was formed into many small dendrite shapes as shown in Figures 10(c). The heat, generated during FSSW process, resulted in small structure formation in SZ in all parameters. No matter how increasing depth of plug or welding time, small grains from precipitation in the SZ at depth of plug 1.5 mm and welding time 30 sec can be observed from Figures 10(e and f). When there were sufficient time and the appropriate heat to stimulate energy, this will result in the growth of grain in TMAZ [26]. This could be explained with Figures 10(g and h) and the hooks were removed.

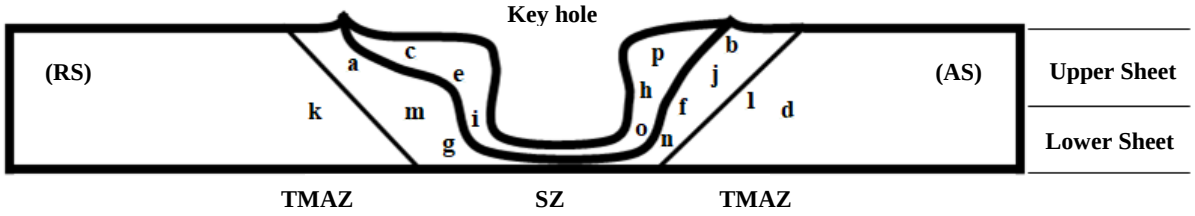

Figure 9 The schematic position model of the microstructure examination

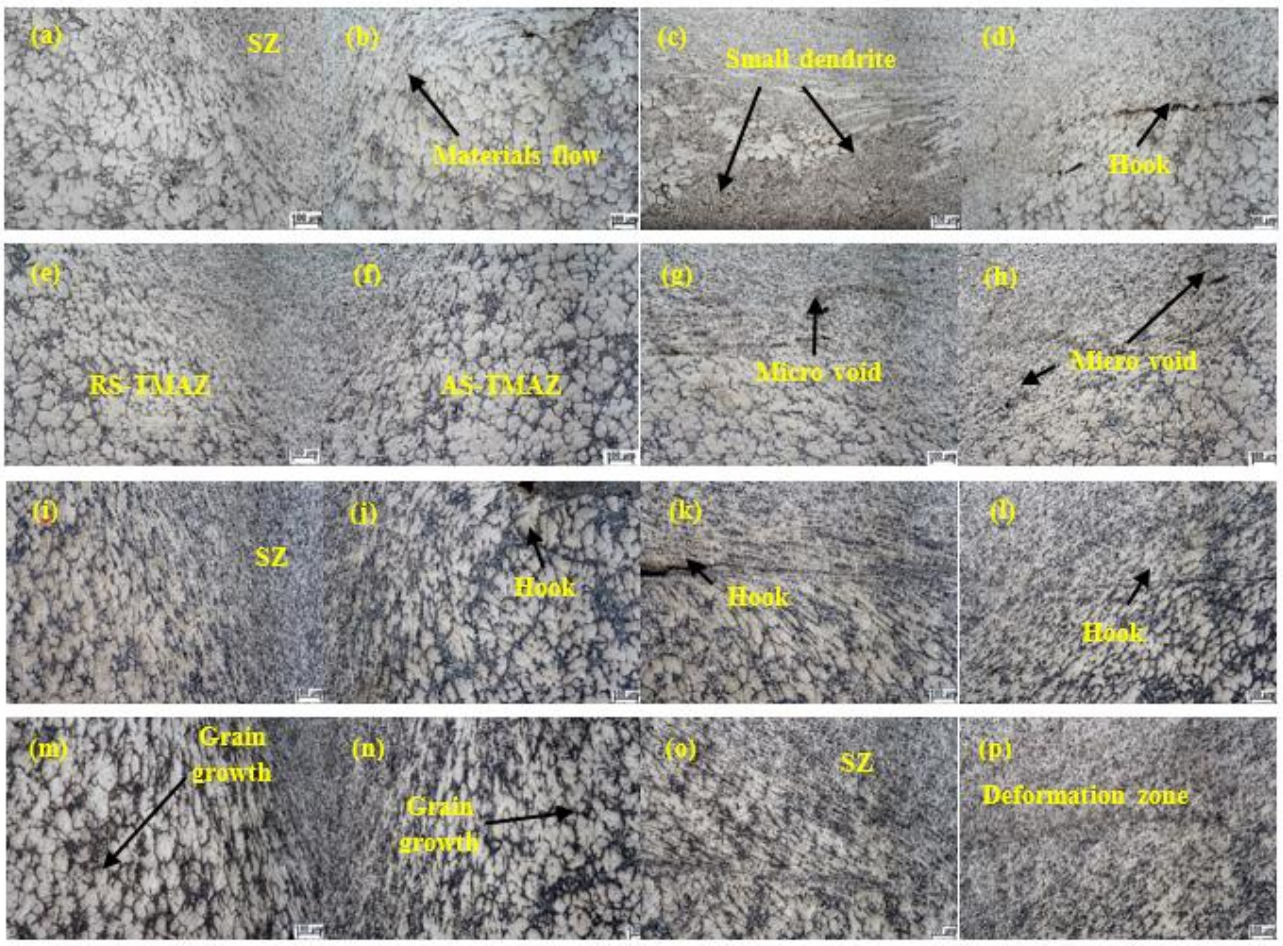

Figure 10 These show microstructure in SZ the rotation speed 380 rpm as: (a-d) depth of plug at 1.0 mm and welding time 30 sec., (e-h) depth of plug at 1.5 mm and welding time 30 sec., (i-l) depth of plug at 1.0 mm and welding time 60 sec., and (m-p) depth of plug at 1.5 mm and welding time 60 sec

Likewise, for the depth of plug at 1.0 mm and welding time at 60 sec shown in Figures 10(i-l), the results show in the same formation of hooks around RS-TMAZ as shown in Figures 10(k), which the RS-TMAZ is the region where the heat is difficult to access. This is why it causes hook defects. On the contrary, the heat in AS-TMAZ highly affects the grain extension. The hook starts with the tear marks in the direction perpendicular to the action force and gets separated until the sample is destroyed [27]. To be noticed that, at depth of plug 1.5 mm and welding time at 60 sec shown in Figures 10(m-p), the hook formation was not observed under this condition. However, the size of α-Al phase in TMAZ has grown significantly from heat and characteristics of grain like-flowers shape, which the growing grain will promote the ductility properties.

At the rotation speed of 1240 rpm, the different characteristics of the microstructure in SZ are shown in Figures 11. The results show that the globular grains in TMAZ are elongated according to the welding rotation direction. The Figures 11(a-d) shows the microstructure at depth of plug at 1.0 mm and welding time at 30 sec, micro voids were found after welding in RS-TMAZ as shown in Figures 11(c), but the hook was found in AS-TMAZ as shown in Figures 11(d). Similarly, increasing welding time from 30 sec to 60 sec with depth of plug at 1.0 mm contributes the hook reduction in TMAZ evaluated from Figures 11(g and h). Figures 11(i-l) shows the microstructure at depth of plug at 1.0 mm and welding time 60 sec. The experimental results show voids in RS-TMAZ and hook in AS-TMAZ shown in Figures 11(k and l). Except other defect, these hooks were the beginning of damage when the tensile was tested which is another reason for the decrease in shear strength [28]. The increase of welding time results in a good tendency of hook and defect. At 60 sec of welding time, hook and defect were not observed. Besides, for longer welding time, coarse grain could be found in near SZ as shown in Figures 11(m-p).

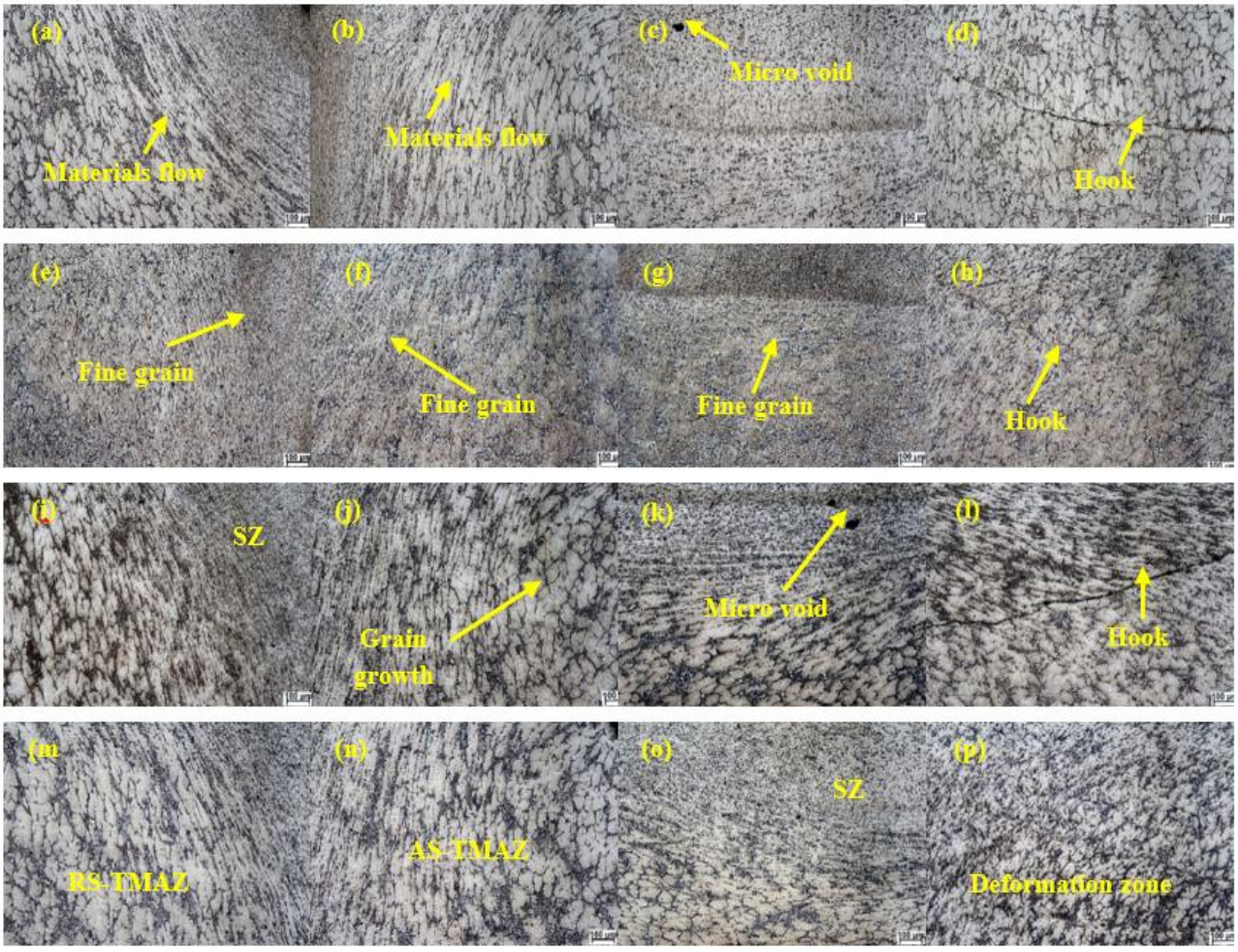

Figure 11 These show microstructure in SZ the rotation speed 1240 rpm as: (a-d) depth of plug at 1.0 mm and welding time 30 sec., (e-h) depth of plug at 1.5 mm and welding time 30 sec., (i-l) depth of plug at 1.0 mm and welding time 60 sec., and (m-p) depth of plug at 1.5 mm and welding time 60 sec

For the rotation speed 2500 rpm shown in Figures 12, these results of the experiment were similar to the rotation speeds of 380 and 1240 rpm. It was found that the destroyed globular grains in SZ caused structural changes shown in Figures 12(a and b), (e and f), (i and j) and (m and n). If the rotation speed is too high, there is a risk of heat loss [29]. It can be noticed that hooks were found in both AS-TMAZ and RS-TMAZ connected along to the SZ, shown in Figures 12(c and d), (g), (k and l) and (o and p) respectively. That is the main reason for the decrease in shear strength explained in the graph (Figure 4) showing the shear strength results. After the results of all experiments were analyzed, the heat occurred during FSSW is related to rotation speed, depth of plug and welding time significantly.

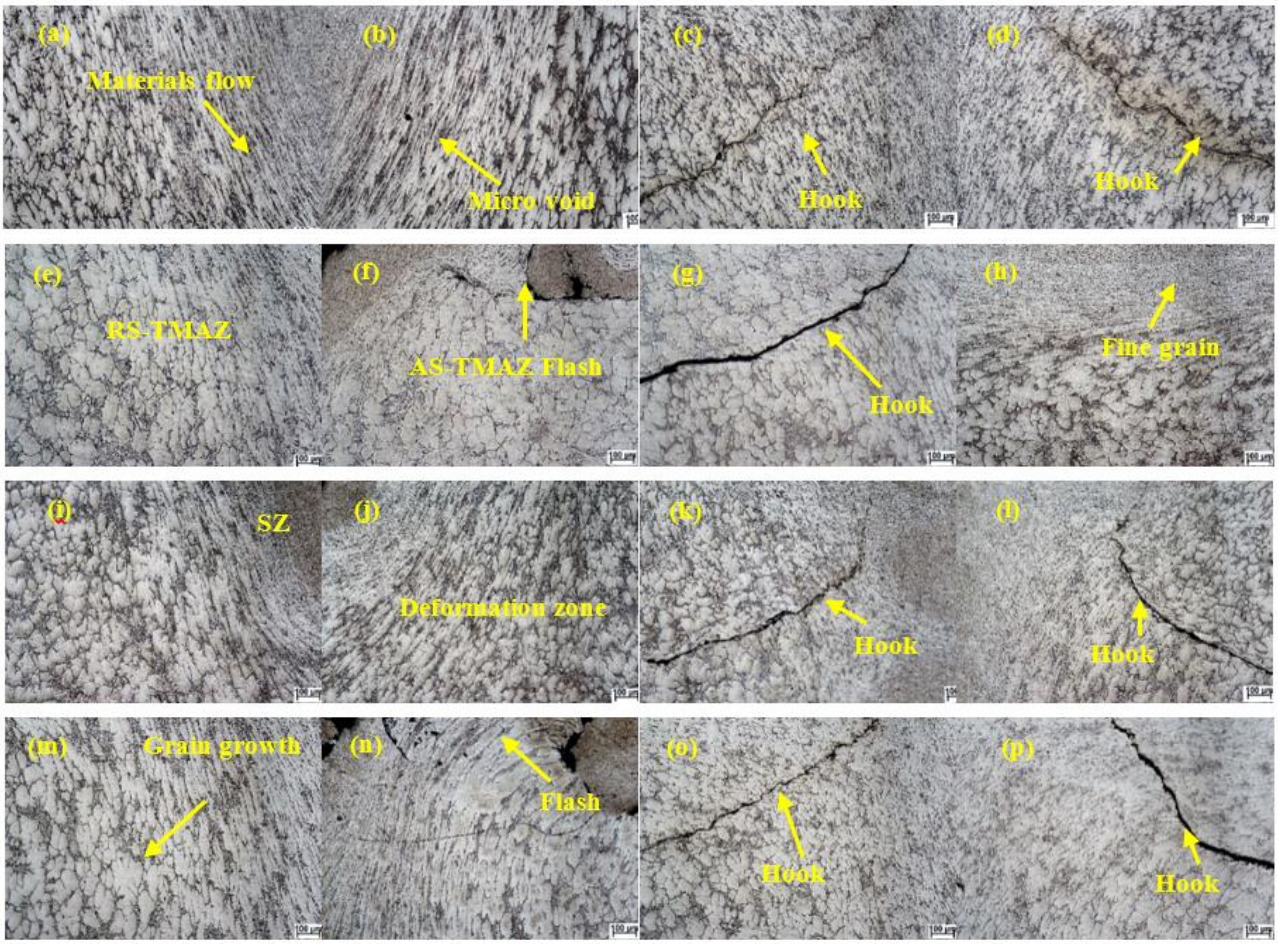

Figure 12 These show microstructure in SZ the rotation speed 2500 rpm as: (a-d) depth of plug at 1.0 mm and welding time 30 sec., (e-h) depth of plug at 1.5 mm and welding time 30 sec., (i-l) depth of plug at 1.0 mm and welding time 60 sec., and (m-p) depth of plug at 1.5 mm and welding time 60 sec

3.4.3 Microstructural results using a scanning electron microscopy

This micrograph is alpha-beta SSM356 aluminum alloys, imaged with 1000x by FEI-Quanta model 450 shown in Figure 13. It illustrates the relationship between the rotational speed, depth of plug, and the welding time on the of β-Mg_2Si phase deformation. The β-Mg_2Si in eutectic phase was formed as a plate-link or cross-link shape with the particle size at 44-49 µm shown in Figure 13(e) and (f). However, the friction force causes the β-Mg_2si phase formation which then becomes a permanent fracture. Such friction force from the rotation speed causes the β-Mg_2si phase to be transformed to β″-Mg_2si phase spreading around the SZ, whose particle size is smaller at 2-7 µm shown in Figure 13(a) and (b), but micro voids can be found after new precipitation. Moreover, a twist of β-Mg_2si phase in the AS-TMAZ resulting in a longitudinal fracture are worm-like shape at 15-21 µm shown in Figure 13d. The microstructure from RS-TMAZ, being affected by the force resulting in β-Mg_2si phase with a rounded fracture, is similar to the microstructure in the SZ at 5-13 µm shown in Figure 13(c). The transformation of β-Mg_2si phase characteristics from the heat during FSSW can be explained as follows:

$$\beta - \mathrm{Mg_2si_{(plate-link\ or\ cross-link)}} \rightarrow \beta' - \mathrm{Mg_2si_{(worm-like)}} \rightarrow \beta'' - \mathrm{Mg_2si_{(precipitation)}}.$$

However, this heat is another cause for β-Mg_2si phase changes. This heat softens the materials by stimulating the movement of atoms. When suitable welding parameters allow materials to precipitate completely, the density of the material after precipitation can be found as small voids since oxygen will penetrate between layers of material. The voids will be the starting point for tearing which could reduce a shear strength and weldability [30].

The Energy-dispersive X-ray spectroscopy (EDS) was analyzed for element mapping in SZ from the rotation speed at 380 rpm, depth of plug at 1.5 mm, and welding time at 60 sec shown in Figure 14(a). The results show a high concentration of 56.82 wt% Al elements, which is the main element of this material as shown in Figure 14(b). It is worth noting that the presence of high oxygen (O) elements at 21.62 wt% was observed. The reason is that the oxygen was inserted during welding into the voids and it has the opportunity to combine with Al to form an aluminum oxide (Al_2O_3), which is not good for mechanical properties [31] shown in Figure 14(d). The silicon (Si) and magnesium (Mg) elements have precipitated from heat. This heat input is the energy that activates the atoms to be moved until the Mg_2Si intermetallic compound was formed, which also promotes the mechanical properties [32]. These elements distributed across the SZ as shown in Figure 14(c and f). the presence of Si element was at 18.63 wt%, Mg element was at 2.66 wt % respectively. There is a small amount of ferrous (F) element at 0.26 wt%. in the SZ due to ferrous has a high melting point. So, it needs higher activation energy to stimulate the movement of atoms, shown in Figure 14(e). The precipitated behavior and varieties of compound elements are an important mechanism for mechanical properties as shown in Table 7.

Table 7 Shows the amount of element around the weld that is analyzed with EDS-Ray spectroscopy

Element	Line Type	Apparent Concentration	k Ratio	Wt.%	Wt.% Sigma	Atomic %
O	K series	1.10	0.00371	21.62	0.32	31.64
F	K series	0.02	0.00013	0.26	0.05	0.25
Mg	K series	0.22	0.00043	2.66	0.28	3.28
Al	K series	4.25	0.03054	56.82	0.31	49.30
Si	K series	0.68	0.00543	18.63	0.18	15.53
Total				100		100

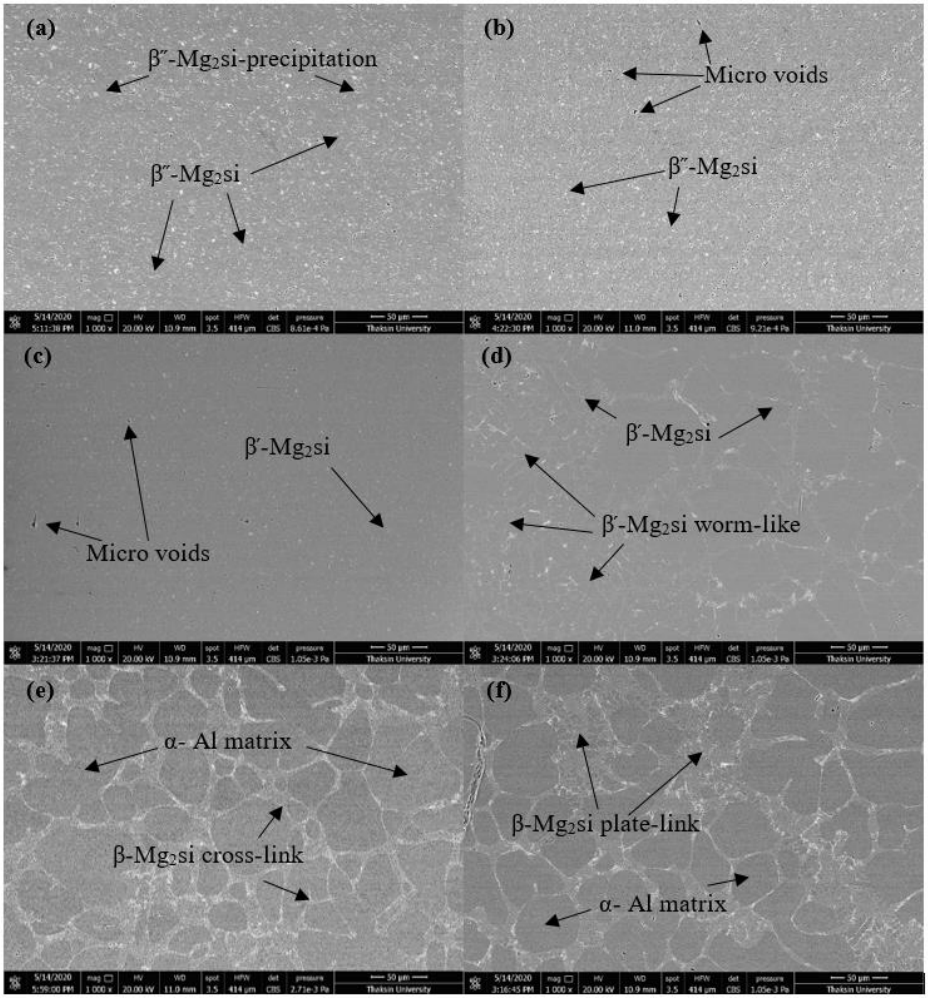

Figure 13 These show microstructure in SZ by SEM at the rotation speed at 380 rpm, depth of plug at 1.5 mm and welding time at 60 sec

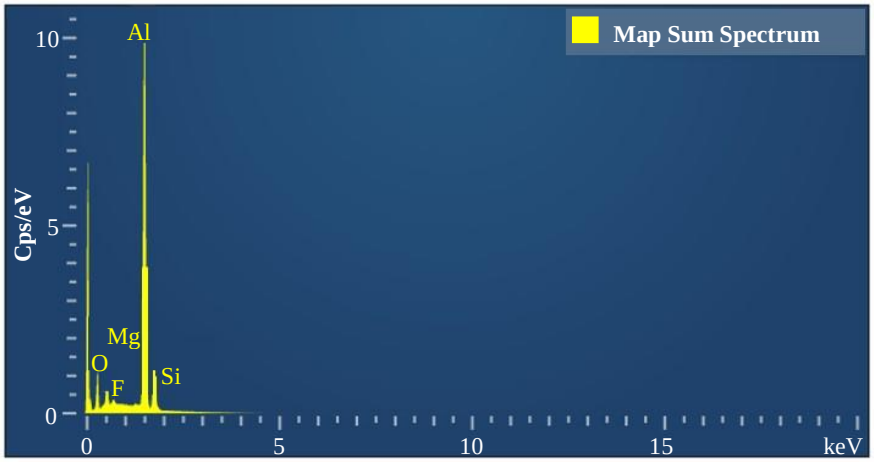

Figure 14 The micrographic element mapping in SZ by EDS-Ray spectroscopy at the rotation speed at 380 rpm, depth of plug at 1.5 mm, and welding time at 60 sec: (a) the presence of SEM micrographs, (b) the presence of aluminum element, (c) the presence of silicon element, (d) the presence of oxygen element, (e) the presence of iron element, and (e) the presence of manganese element.

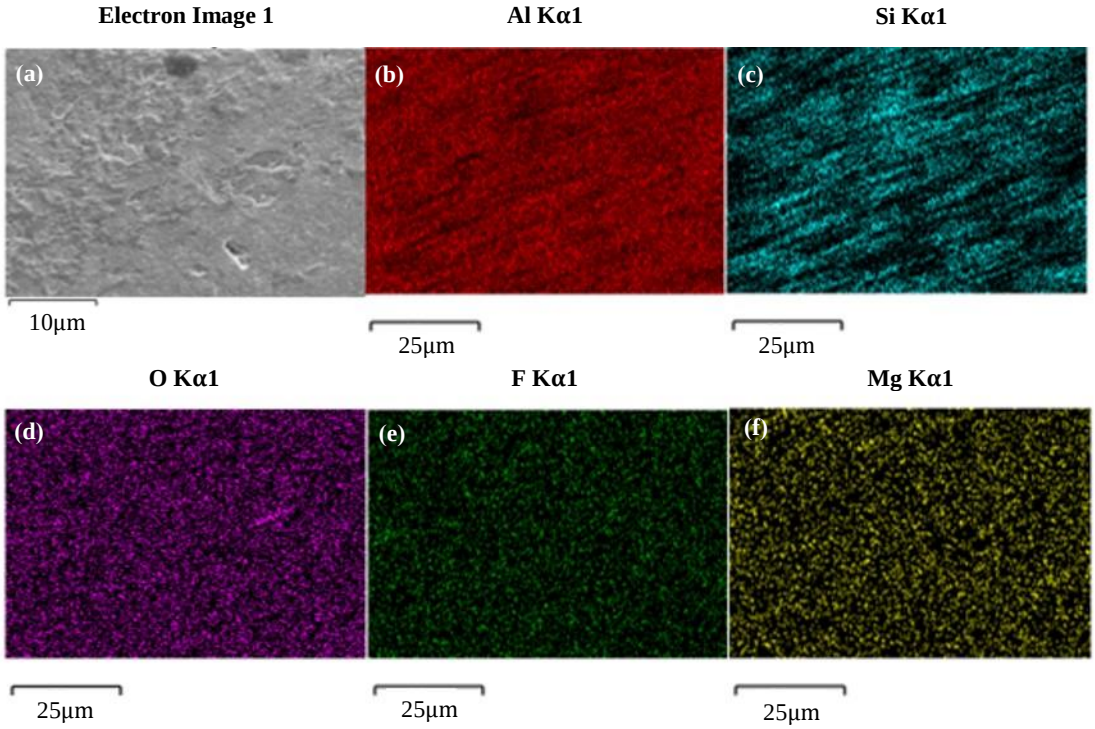

Figure 14 (continued) The micrographic element mapping in SZ by EDS-Ray spectroscopy at the rotation speed at 380 rpm, depth of plug at 1.5 mm, and welding time at 60 sec: (a) the presence of SEM micrographs, (b) the presence of aluminum element, (c) the presence of silicon element, (d) the presence of oxygen element, (e) the presence of iron element, and (e) the presence of manganese element.

4. Conclusions

It is clearly seen that there is a possibility to successfully achieve SSM 356 aluminum alloy with FSSW method with good shear strength and good mechanical properties. The optimum parameters were rotation speed at 380 rpm, depth of plug 1.5 mm, and welding time at 60 sec. This provides the average shear strength value at 174.2 MPa (92.12 percent of joint efficiency compared with the base metal). The highest hardness values in SZ was around 60-65 HV. The confidence level of analyzed experimental design was 95.00% (α=0.05), coefficient of R^2 at 0.96, which could create precise shear tensile model equations. For the metallurgy in SZ, there is a transformation from a globular structure to a fine structure. For AS-TMAZ and RS-TMAZ, a globular structure is elongated into a grain-like structure. For some parameters, the hook defects were found. The characteristics of β-Mg2si phase in SZ show precipitations behavior and transform to be β″-Mg2si phase, which causes the particle size to become smaller around 2-7 µm. When analyzing the distribution of elements, it shows that Al, Si, Mg, and F generally distribute around the SZ, but the high volume of oxygen (O) penetrates into the voids occurring after FSSW of SSM 356 aluminum alloys.

5. Acknowledgements

The author would like to thank the Faculty of Industrial Technology, Songkhla Rajabhat University, and GISCO Company Limited., in Thailand for providing materials for this research work.

6. References

[1] Chainarong S, Muangjunburee P, Suthummanon S. Friction stir processing of SSM356 aluminium alloy. Procedia Eng. 2014;97:732-40.
[2] Chen YC, Gholinia A, Prangnell PB. Interface structure and bonding in abrasion circle friction stir spot welding: a novel approach for rapid welding aluminium alloy to steel automotive sheet. Mater Chem Phys. 2012;134(1):459-63.
[3] Wannasin J, Martinez RA, Flemings MC. Grain refinement of an aluminum alloy by introducing gas bubbles during solidification. Scr Mater. 2006;55(2):115-8.
[4] Yang X, Fu T, Li W. Friction stir spot welding: a review on joint macro and microstructure, property, and process modelling. Adv Mater Sci Eng. 2014;2014(1):1-11.
[5] Gao C, Gao R, Ma Y. Microstructure and mechanical properties of friction spot welding aluminium-lithium 2A97 alloy. Mater Des. 2015;83:719-27.
[6] Thomas WM. Friction stir welding of ferrous materials; a feasibility study. Steel World. 1999;4(2):55-9.
[7] Rao HM, Yuan W, Badarinarayan H. Effect of process parameters on mechanical properties of friction stir spot welded magnesium to aluminum alloys. Mater Des. 2015;66:235-45.
[8] Li W, Li J, Zhang Z, Gao D, Wang W, Dong C. Improving mechanical properties of pinless friction stir spot welded joints by eliminating hook defect. Mater Des. 2014;62:247-54.
[9] Tozaki Y, Uematsu Y, Tokaji K. A newly developed tool without probe for friction stir spot welding and its performance. J Mater Process Technol. 2010;201(6-7):844-51.

[10] Sitthipong S, Towatana P, Meengam C, Chainarong S, Muangjunburee P. The influence of parameters affecting mechanical properties and microstructures of semi-solid-metal 7075 aluminum alloy by using friction stir spot welding. Eng J. 2018;22(3): 51-64.
[11] Liu H, Zhao Y, Su X, Yu L, Hou J. Microstructural characteristics and mechanical properties of friction stir spot welded 2A12-T4 aluminum alloy. Adv Mater Sci Eng. 2013;2013:1-10.
[12] Fereiduni E, Movahedi M, Kokabi AH. Aluminum/steel joints made by an alternative friction stir spot welding process. J Mater Process Technol. 2015;224:1-10.
[13] Lakshminarayanan A, Annamalai V, Elangovan K. Identification of optimum friction stir spot welding process parameters controlling the properties of low carbon automotive steel joints. J Mater Res Technol. 2015;4(3):267-72.
[14] Urso GD. Thermo-mechanical characterization of friction stir spot welded AA6060 sheets: experimental and FEM analysis. J Manuf Process. 2015;17:108-19.
[15] Burapa R, Janudom S, Chucheep T, Canyook R, Wannasin J. Effects of primary phase morphology on mechanical properties of Al-Si-Mg-Fe alloy in semi-solid slurry casting process. Trans Nonferrous Met Soc China. 2010;20:s857-61.
[16] Lin YC, Chen JN. Influence of process parameters on friction stir spot welded aluminum joints by various threaded tools. J Mater Process Technol. 2015;225:347-56.
[17] Chainarong S, Meengam C, Tehyo M. Rotary friction welding of dissimilar joints between SSM356 and SSM6061 aluminium alloys produced by GISS. Eng J. 2017;21(1):181-91.
[18] Cao JY, Wang M, Kong L, Guo LJ. Hook formation and mechanical properties of friction spot welding in alloy 6061-T6. J Mater Process Technol. 2016;230:254-63.
[19] Martinez N, Kumar N, Mishra RS, Doherty K. Microstructural variation due to heat gradient of a thick friction stir welded aluminum 7449 alloy. J Alloy Comp. 2017;713:51-6.
[20] Meengam C, Chainarong S, Muangjunburee P. Friction welding of semi-solid metal 7075 aluminum alloy. Mater Today Proc. 2017;4(2):1303-11.
[21] Baratzadeh F, Boldsaikhan E, Nair R, Burford D, Lankarani H. Investigation of mechanical properties of AA6082-T6/AA6063-T6 friction stir lap welds. J Adv Join Process. 2020;1:100011.
[22] Dong H, Chen S, Song Y, Guo X, Zhang X, Sun Z. Refilled friction stir spot welding of aluminum alloy to galvanized steel sheets. Mater Des. 2016;94:457-66.
[23] Plaine AH, Suhuddin UFH, Afonso CRM, Alcantara NG, dos Santos JF. Interface formation and properties of friction spot welded joints of AA5754 and Ti6Al4V alloys. Mater Des. 2016;93:224-31.
[24] Andrade DG, Leitao C, Rodrigues DM. Influence of base material characteristics and process parameters on frictional heat generation during friction stir spot welding of steels. J Manuf Process. 2019;43:98-104.
[25] Shena Z, Li W, Ding Y, Hou W, Xiu XC, Guo W, et al. Material flow during refill friction stir spot welded dissimilar al alloys using a grooved tool. J Manuf Process. 2020;49:260-70.
[26] Vacchi GS, Silva R, Plaine AH, Suhuddin UFH, Alcantara NG, Sordi VL, et al. Refill friction stir spot welded AA5754-H22/Ti-6Al-4V joints: microstructural characterization and electrochemical corrosion behavior of aluminum surfaces. Mater Today Proc. 2020;22:110759.
[27] Yin YH, Sun N, North TH, Hu SS. Hook formation and mechanical properties in AZ31 friction stir spot welds. J Mater Process Technol. 2010;210(14):2062-70.
[28] Silva BH, Suhuddin U, Zepon G, Bolfarini C, dos Santos JF. Refill friction stir spot welding of AA6082-T6 alloy: hook defect formation and its influence on the mechanical properties and fracture behavior. Mater Sci Eng. 2020;773:138724.
[29] Li G, Zhou L, Luo L, Wu X, Guo N. Microstructural evolution and mechanical properties of refill friction stir spot welded alclad 2A12-T4 aluminum alloy. J Mater Res Technol. 2019;8(5):4115-29.
[30] Evans W, Neely K, Strauss A, Cook GE. Weldability of an iron meteorite by friction stir spot welding: a contribution to in-space manufacturing. Acta Astronautica. 2017;140:452-8.
[31] Park ID, Lee CT, Kim HS, Choi WJ, Kang MC. Structural considerations in friction welding of hybrid Al2O3-reinforced aluminum composites. Trans Nonferrous Met Soc China. 2011;21:s41-6.
[32] Sonomura H, Ozaki T, Katagiri K, Hasegawa Y, Tanaka T, Kakitsuji A. Lap joint formed by friction stir spot welding between SiC and magnesium alloy containing aluminum. Ceram Int. 2020;46(6):7654-8.